

A. Gregory Sorensen, MD  
Ona Wu, MS  
William A. Copen, AM  
Timothy L. Davis, PhD  
R. Gilberto Gonzalez, MD,  
PhD  
Walter J. Koroshetz, MD  
Timothy G. Reese, PhD  
Bruce R. Rosen, MD, PhD  
Van J. Wedeen, MD  
Robert M. Weisskoff, PhD

**Index terms:**

Anisotropy  
Brain, diffusion, 10.12144, 10.92  
Brain, infarction, 10.78  
Brain, ischemia, 10.781  
Brain, MR, 10.121411, 10.12144  
Diffusion tensor  
Magnetic resonance (MR), diffusion study, 10.12144, 10.92  
Magnetic resonance (MR), echo planar, 10.121412, 10.12144

**Radiology 1999; 212:785-792**

**Abbreviations:**

ADC = apparent diffusion coefficient  
CNR = contrast-to-noise ratio  
ROI = region of interest  
SNR = signal-to-noise ratio

<sup>1</sup> From the Departments of Radiology (A.G.S., O.W., W.A.C., T.L.D., R.G.G., T.G.R., B.R.R., V.J.W., R.M.W.) and Neurology (W.J.K.), Massachusetts General Hospital and Harvard Medical School, Neuroradiology Section and MGH-NMR Center, Mailcode CNY 149-2301, Boston, MA 02119. Received April 13, 1998; revision requested June 30; revision received November 24; accepted March 29, 1999. **Address reprint requests to** A.G.S. (e-mail: [sorensen@nmr.mgh.harvard.edu](mailto:sorensen@nmr.mgh.harvard.edu)).

© RSNA, 1999

**Author contributions:**

Guarantor of integrity of entire study, A.G.S.; study concepts and design, A.G.S., O.W., B.R.R., R.M.W.; definition of intellectual content, A.G.S., O.W., T.L.D., T.G.R., B.R.R., V.J.W., R.M.W.; literature research, A.G.S., O.W.; clinical studies, A.G.S., R.G.G., W.J.K.; experimental studies, A.G.S., O.W., T.L.D., T.G.R., B.R.R., V.J.W., R.M.W.; data acquisition, A.G.S., R.G.G., W.J.K.; data analysis, A.G.S., O.W., W.A.C., T.L.D., B.R.R., R.M.W.; statistical analysis, A.G.S., O.W., W.A.C., B.R.R., R.M.W.; manuscript preparation, A.G.S., O.W., T.L.D.; manuscript editing and review, all authors.

# Human Acute Cerebral Ischemia: Detection of Changes in Water Diffusion Anisotropy by Using MR Imaging<sup>1</sup>

**PURPOSE:** To (a) determine the optimal choice of a scalar metric of anisotropy and (b) determine by means of magnetic resonance imaging if changes in diffusion anisotropy occurred in acute human ischemic stroke.

**MATERIALS AND METHODS:** The full diffusion tensor over the entire brain was measured. To optimize the choice of a scalar anisotropy metric, the performances of scalar indices in simulated models and in a healthy volunteer were analyzed. The anisotropy, trace apparent diffusion coefficient (ADC), and eigenvalues of the diffusion tensor in lesions and contralateral normal brain were compared in 50 patients with stroke.

**RESULTS:** Changes in anisotropy in patients were quantified by using fractional anisotropy because it provided the best performance in terms of contrast-to-noise ratio as a function of signal-to-noise ratio in simulations. The anisotropy of ischemic white matter decreased ( $P = .01$ ). Changes in anisotropy in ischemic gray matter were not significant ( $P = .63$ ). The trace ADC decreased for ischemic gray matter and white matter ( $P < .001$ ). The first and second eigenvalues decreased in both ischemic gray and ischemic white matter ( $P < .001$ ). The third eigenvalue decreased in ischemic gray ( $P = .001$ ) and white matter ( $P = .03$ ).

**CONCLUSION:** Gray matter is mildly anisotropic in normal and early ischemic states. However, early white matter ischemia is associated with not only changes in trace ADC values but also significant changes in the anisotropy, or shape, of the water self-diffusion tensor.

Magnetic resonance (MR) imaging has excelled at depicting the macroscopic anatomy of the human brain. However, many normal cellular functions and disease processes that occur at the microscopic level do not affect conventional MR relaxation parameters. As a result, certain disease processes such as early acute cerebral ischemia are poorly assessed with conventional MR imaging. Routine diagnosis could be improved if MR imaging could be used to investigate events at the microscopic level; this has been shown to be possible with acute ischemic stroke, for which diffusion- and perfusion-weighted MR imaging have been used to document abnormalities, even when conventional MR imaging shows no abnormality (1-3).

To date, most diffusion imaging of humans in a clinical environment has been used to measure either a single direction of the diffusion tensor (1,2,4-12) or the trace of the diffusion tensor (1,3,13-18). Several studies (19-24) have documented marked anisotropy in the normal human brain, particularly in regions of white matter. However, to our knowledge, in only a few studies (25,26) has the full diffusion tensor been measured. Studies (26,27) sampling the full diffusion tensor in patients with chronic stroke have found changes in anisotropy values in infarcted tissue compared with those for normal contralateral tissue. In addition, with use of the full diffusion tensor, chronic changes in tensor orientation were measured in a patient who had an embolic infarct (27).

On the basis of evidence of changes in anisotropy in patients with chronic stroke, we hypothesize that changes in anisotropy will also occur in cases of acute cerebral ischemia,

particularly in white matter. Measuring the entire diffusion tensor during ischemia may thus provide insight regarding the mechanisms involved in acute ischemia and could improve diagnosis. In two earlier studies (28,29) in which middle cerebral arterial occlusion in cats was used, changes in anisotropy were not detected 15 hours after occlusion. However, in one study (30) in which middle cerebral arterial occlusion in rats was used, a reduction in anisotropy 24–48 hours after occlusion was measured. In none of these studies was the full diffusion tensor sampled. We sought to investigate changes in anisotropy in white matter and gray matter in human acute cerebral ischemia. We hypothesize that acute ischemic tissue, in particular areas normally anisotropic, such as white matter, will show changes in anisotropy compared with tissue in its normal state.

The diffusion tensor has six independent components, and therefore, the choice of the optimal way to view changes in the shape of the tensor is not obvious. Furthermore, if changes are to be measured and quantified, some type of metric, preferably a scalar metric rather than a vector or tensor metric, must be used. To visualize and to quantify changes in anisotropy during ischemia, we chose to evaluate and use scalar metrics. Because measurement of diffusion anisotropy can be complicated by the presence of noise (31), we first used Monte Carlo simulations and data from a healthy human volunteer to validate our metrics. We then applied our metrics to investigate changes during ischemia.

The Materials and Methods section of this article is divided into two parts. In the first section, Technical Development, we describe our implementation of diffusion tensor imaging and our evaluation of scalar metrics of anisotropy. In the second section, Human Acute Cerebral Ischemia, we describe the application of full-tensor imaging to human acute cerebral ischemia.

## MATERIALS AND METHODS

Institutional review board approval and informed consent were obtained for our study.

### Technical Development

Diffusion is the random translational motion of molecules owing to thermal energy. The diffusion process in three-dimensional space can be characterized

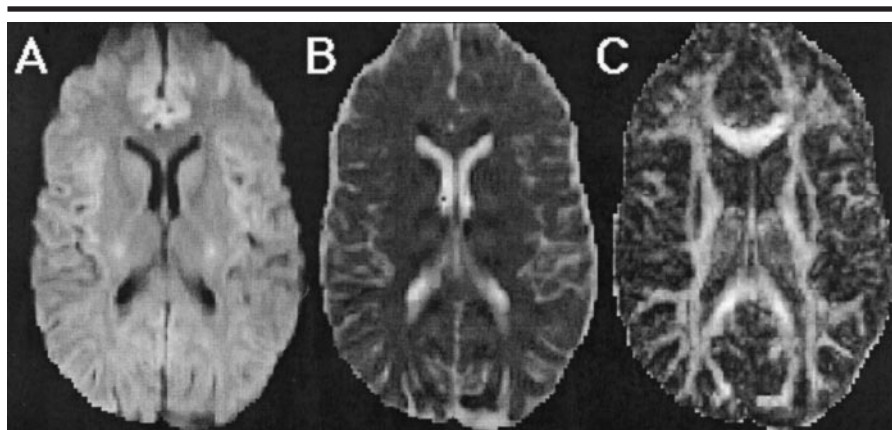


**Figure 1.** Images obtained axially in the healthy volunteer with use of 30 repetitions that resulted in an estimated SNR of 65. The SNR of our typical full-head diffusion tensor data set is 20. The imaging parameters were 6,000/118 (repetition time msec/echo time msec) with a  $b$  value of 1,221 sec/mm<sup>2</sup>. A, Isotropic (trace) diffusion-weighted image. B, Mean trace ADC map. C, Fractional anisotropy map.

by a symmetric tensor because its rate is direction-dependent and symmetric. This tensor has six degrees of freedom and thus can be represented by  $D$ , a  $3 \times 3$  symmetric matrix (vector and tensor quantities are denoted in boldface). In isotropic media,  $D$  reduces to an identity matrix scaled by a constant,  $D$ , because the rate of diffusion is independent of direction, meaning that the probability that a particle moves to another point follows the behavior of a spherically symmetric Gaussian function (32). However, in the case of restricted diffusion, the diffusing particles encounter barriers that are direction dependent. The probability that a particle will move to another point then becomes a function of the geometry of the diffusion barriers (33) and results in diffusion coefficients that are anisotropic or direction dependent.

To measure the full diffusion tensor on a voxel-by-voxel basis, we used the pulsed field gradient method described by Stejskal and Tanner (34) by using seven measurements. The tensor was sampled by using a T2-weighted one-shot echo-planar imaging technique (35) repeated in seven different directions, which is the minimum required for solving for the diffusion coefficients that characterizes the diffusion tensor (36–39). Imaging was performed on a 1.5-T MR instrument with 5.4.2 software (Signa; GE Medical Systems, Milwaukee, Wis) and echo-planar imaging capabilities by means of a hardware upgrade (ANMR, Wilmington, Mass), including the “catch and hold” modification. We used T2-weighted single-shot pulsed field gradient spin-echo sequences that consisted of diffu-

sion encoding pulses of a duration ( $\theta$ ) of 47 msec, with an interpulse temporal offset ( $\Delta$ ) of 52 msec, placed symmetrically about the 180° radio-frequency pulse. With catch-and-hold enabled, the echo time was 118 msec. We used a repetition time of 6,000 msec and obtained up to 20 axial sections with a 6-mm section thickness and a 1-mm spacing between sections. A fixed field of view of 40 × 20 cm and an acquisition matrix of 256 × 128 pixels were used. A single complete tensor acquisition required 42 seconds for imaging all sections.

Three full-head diffusion tensor samples typically were acquired and then averaged with a resultant signal-to-noise ratio (SNR) of approximately 20 in a total acquisition time of 126 seconds. The SNR was estimated from nondiffusion-weighted images after averaging by calculating the ratio of the mean signal intensity of a 5 × 5 region of interest (ROI) in the thalamus to the SD of the noise measured in background areas outside the head that were artifact free. A healthy 34-year-old man underwent imaging with an estimated SNR of 65 by using 30 full diffusion tensor samples for one axial section, with a total acquisition time of 21 minutes.

Diffusion gradients were applied in turn at  $r_0 = (x, y, z) = (0.05, 0.05, 0.0)$  (a finite low  $b$  value rather than a  $b$  value of zero was used to avoid image artifacts) and the six  $r_i = \{(1, 1, 0), (1, -1, 0), (0, 1, 1), (0, -1, 1), (1, 0, 1), (-1, 0, 1)\}$  G/cm, which corresponded to the centers of the non-opposed edges of a cube. The approximate  $b$  value, where  $b$  is a measure of diffusion weighting (4), was 1,221 sec/mm<sup>2</sup> for each of the six directions and 3

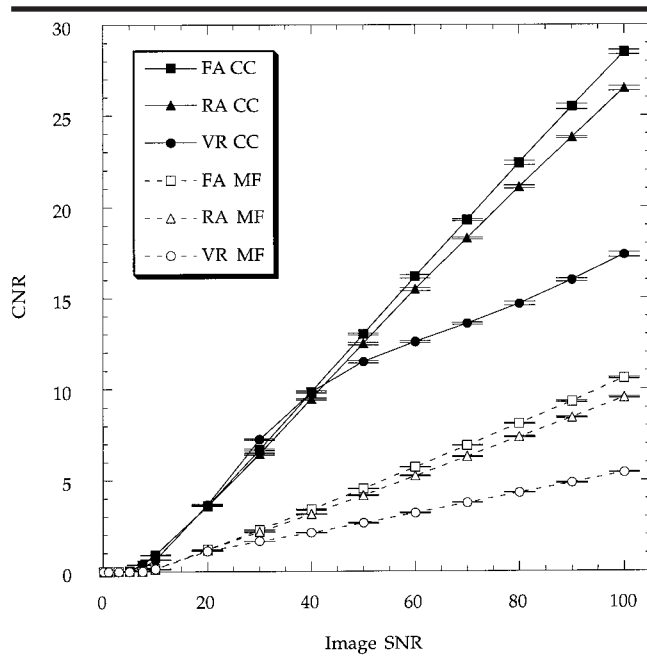


**Figure 2.** Graph shows CNR as a function of SNR for fractional anisotropy (FA), relative anisotropy (RA), and volume ratio (VR) indices computed from Monte Carlo simulations of two tissue types with different levels of anisotropy. The eigenvalues for the two tissue types were based on in vivo measurements of the splenium of the corpus callosum (CC) and the left forceps major (MF) in the healthy volunteer who underwent imaging with 30 repetitions instead of three and whose data are shown in Figure 1. The corpus callosum had eigenvalues of 1.7, 0.3, and  $0.1 \times 10^{-3}$  mm<sup>2</sup>/sec, and the left forceps major had eigenvalues of 1.2, 0.9, and  $0.3 \times 10^{-3}$  mm<sup>2</sup>/sec. The error bars represent the SD in computed CNR over 10 different simulations.

sec/mm<sup>2</sup> for the image obtained with a low  $b$  value. A unique solution for  $D$  can be obtained provided the  $3 \times 3$  symmetric matrices,  $[r_i \ r_i^T]$ ,  $i = 1, \dots, 6$ , are linearly independent. In our calculations, we also included the effects of the imaging gradients in which techniques were used similar to those previously described (32–34). In addition, we corrected for eddy-current warping artifacts.

Once the diffusion tensor coefficients were computed, the diffusion tensor's eigenvalues,  $\lambda_i$ , and eigenvectors were calculated. The eigenvectors of the symmetric diffusion tensor, a set of orthogonal vectors, defined the orientation of the principal axes of the diffusion tensor ellipsoid in space. Their corresponding eigenvalues represent the lengths of the axes. These quantities therefore defined the size and shape of the ellipsoids of  $D$  and are independent of its orientation in its frame of measurement. From these eigenvalues, coordinate independent scalar functions of  $D$  were constructed that measured its degree of anisotropy.

A challenge to measuring anisotropy from the computed eigenvalues arises

from noise contamination (31). For example, even in an isotropic sample, noise will make the computed eigenvalues unequal, with the resultant implication of some anisotropy. For anisotropy metrics that rely on sorting of the eigenvalues, a bias and a variance that depend on the diffusion properties of the tissue have been demonstrated (31). Therefore, in this study, we limited our evaluation of anisotropy metrics to intravoxel scalar indices (25,31,40) that did not require the sorting of eigenvalues.

We computed maps of fractional anisotropy, relative anisotropy, and volume ratio indices. Fractional anisotropy (FA), the ratio of the anisotropic component of the diffusion tensor to the whole diffusion tensor, is defined (40) as

$$FA(D) = \sqrt{\frac{3}{2} \frac{\sqrt{(\lambda_1 - \langle D \rangle)^2 + (\lambda_2 - \langle D \rangle)^2 + (\lambda_3 - \langle D \rangle)^2}}{\sqrt{\lambda_1^2 + \lambda_2^2 + \lambda_3^2}}},$$

with  $\langle D \rangle = \frac{1}{3}(\lambda_1 + \lambda_2 + \lambda_3)$ , which is the trace apparent diffusion coefficient (ADC), or mean diffusivity. Relative anisotropy

(RA), the ratio of the variance of the computed eigenvalues to their mean, is defined (40) to be

$$RA(D) = \sqrt{\frac{1}{3} \frac{\sqrt{(\lambda_1 - \langle D \rangle)^2 + (\lambda_2 - \langle D \rangle)^2 + (\lambda_3 - \langle D \rangle)^2}}{\langle D \rangle}}.$$

Volume ratio (VR), the ratio of the volume of the diffusion tensor ellipsoid to the volume of a sphere in which the radius is the mean diffusivity, is defined (31) as

$$VR(D) = 1 - \frac{\lambda_1 \lambda_2 \lambda_3}{\langle D \rangle^3}.$$

We compared these scalar diffusion anisotropy metrics by using Monte Carlo methods to simulate diffusion-weighted images over a range of SNRs of 0.1–100. Anisotropy maps were generated by using the three metrics described, and the contrast-to-noise ratio (CNR) between the anisotropic and isotropic region was computed. The CNR was defined as

$$CNR = \frac{|\bar{x} - \bar{y}|}{\sqrt{\sigma_x^2 + \sigma_y^2}},$$

where  $x$  and  $y$  are computed anisotropy values for anisotropic and isotropic media, respectively, and  $\sigma_x$  and  $\sigma_y$  are their SDs.

The diffusion-weighted images were simulated by using eigenvalues measured in a healthy volunteer. The mean of 30 diffusion tensor data sets was used to increase the SNR of the acquired diffusion images to approximately 65. We outlined  $2 \times 2$  ROIs in two homogeneous white matter regions—the splenium of the corpus callosum and the left forceps major. The measured mean eigenvalues, 1.7, 0.3, and  $0.1 \times 10^{-3}$  mm<sup>2</sup>/sec in the corpus callosum and 1.2, 0.9, and  $0.3 \times 10^{-3}$  mm<sup>2</sup>/sec in the left forceps major were used in Monte Carlo simulations to synthesize diffusion-weighted images. The simulated diffusion-weighted images consisted of  $128 \times 128$ -pixel regions of anisotropic white matter media and  $128 \times 128$ -pixel regions of isotropic media. For the isotropic media, eigenvalues of 0.8, 0.8, and  $0.8 \times 10^{-3}$  mm<sup>2</sup>/sec were used because they were representative of values measured in cortical gray matter and also matched values reported by another group (31). The mean and SD of each anisotropy measure as a function of image SNR were then calculated.

The CNR between the white matter regions and the isotropic regions was computed for SNR levels of 0.1–100.0. The

SNR was varied by changing the statistical characteristics of the noise added to the real and imaginary components of the noise-free diffusion-weighted images (31,41). These random noise values were normally distributed with a mean of zero and different variances, depending on the desired SNR. The simulated acquired signal was taken to be the magnitude of the complex images. These steps were repeated 10 times to assess the variability of results between different simulations. In addition, Monte Carlo simulations were used to estimate the contribution of noise bias and variance to the computed eigenvalues.

To investigate the variability of ADC and anisotropy metrics between different imaging sessions in the same subject, the same healthy 34-year-old male volunteer underwent imaging three times in three separate sessions, with a resultant total of nine full-head tensor data sets. The trace ADC values, anisotropy index values, and eigenvalues were calculated by using  $2 \times 2$  ROIs. The mean and SD of ADC and anisotropy values in ROIs placed in deep gray matter, or thalamus; deep white matter, or corpus callosum; and cerebrospinal fluid, or atrium of the right lateral ventricle, were calculated.

### Human Acute Cerebral Ischemia

**Patient recruitment.**—Patients who presented with symptoms of acute cerebral ischemia underwent imaging with an acute stroke protocol similar to published techniques (3). The protocol included evaluation by the hospital stroke service, computed tomographic scanning, and MR imaging, which may involve both diffusion- and, at the radiologist's and neurologist's discretion, perfusion-weighted functional MR imaging. For this study, patients were selected at random from patients with acute stroke who underwent full diffusion tensor imaging. This study included only patients who underwent imaging less than 24 hours after they were last known to be asymptomatic.

All patients underwent full diffusion tensor imaging averaged over three data sets for a total acquisition time of 126 seconds. Isotropic diffusion-weighted images were calculated by taking the geometric mean of the six images obtained with a  $b$  value of 1,221 sec/mm<sup>2</sup>. No head restraints or navigator echoes were used to control or correct for patient motion. Patients were excluded if the data contained image artifacts due to motion or other technical reasons. Patients were excluded if their isotropic diffusion-

**TABLE 1**  
Stability of Mean of the ADC, Fractional Anisotropy, and Eigenvalue Measurements

Measurement*	Thalamus	Splenium	Cerebrospinal Fluid
ADC	0.72 (0.05)	0.62 (0.07)	2.46 (0.08)
FA	0.37 (0.04)	0.84 (0.04)	0.19 (0.03)
$\lambda_1$	1.00 (0.08)	1.43 (0.13)	2.94 (0.14)
$\lambda_2$	0.70 (0.06)	0.30 (0.08)	2.41 (0.11)
$\lambda_3$	0.45 (0.05)	0.12 (0.04)	2.03 (0.07)

Note.—Stability of gray and white matter measurements of the ADC, fractional anisotropy, and eigenvalues in nine separate scanning sessions in the same volunteer at three imaging acquisitions at three different dates;  $2 \times 2$  ROIs were placed for each study in the thalamus, the splenium of the corpus callosum, and the cerebrospinal fluid (atrium of the right lateral ventricle). Data are the mean of the ROIs for the nine images. Numbers in parentheses are the SD.

\* FA = fractional anisotropy. The units of ADC,  $\lambda_1$ ,  $\lambda_2$ , and  $\lambda_3$  are in  $10^{-3}$  mm<sup>2</sup>/sec. Fractional anisotropy values are unitless.

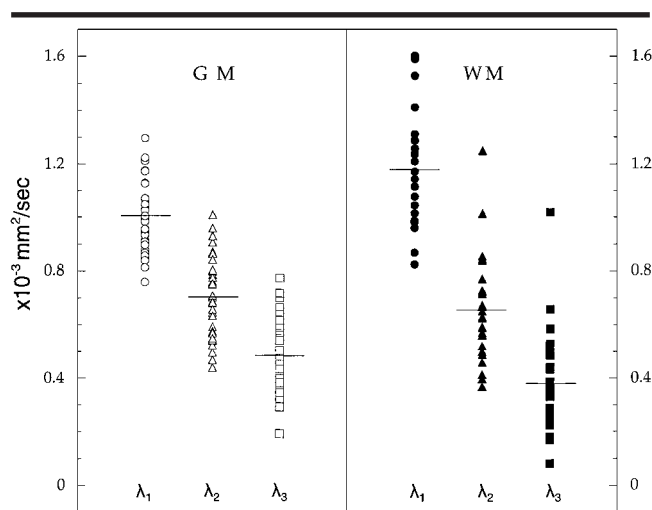


**Figure 3.** Graph shows eigenvalues in normal contralateral regions of the brain in patients with acute ischemia. The horizontal lines indicate the sample means. Normal mean  $\lambda_1$ ,  $\lambda_2$ , and  $\lambda_3$  values are all significantly different from each other for both gray matter (GM) and white matter (WM) ( $P < .001$ ).

weighted image was normal. Patients were also excluded if the time of onset of symptoms was not available or determinable to be less than 24 hours or if follow-up imaging to confirm the infarct was not available. Fifty patients (33 men, 17 women; age distribution, 62.9 years  $\pm$  21 [mean  $\pm$  SD]) met our selection criteria, and there were 25 white matter infarcts and 35 gray matter infarcts. Ten patients had lesions in both gray and white matter. The mean time and SD to imaging from the time the patient was last seen to be healthy was 7.8 hours  $\pm$  3.7.

**Data analysis.**—For the purpose of this work, the ischemic focus was defined as the area of hyperintensity on the initial trace diffusion-weighted images and was confirmed by comparison with follow-up

images. We placed the following  $2 \times 2$  ROIs: ischemic gray matter, contralateral normal-appearing gray matter, ischemic white matter, and contralateral normal-appearing white matter. In the ischemic regions, the ROIs were placed in the geometric center. Care was taken that the same type of gray or white matter (eg, deep or cortical) was chosen in the contralateral hemisphere as in the ischemic focus. If the lesion did not involve both gray and white matter as determined by the neuroradiologist (A.G.S.), then only the appropriate ROI and its corresponding contralateral ROI were placed. The areas chosen as normal were also confirmed to be normal at follow-up examinations. The mean and SD for trace ADC and anisotropy values were obtained for each ROI.

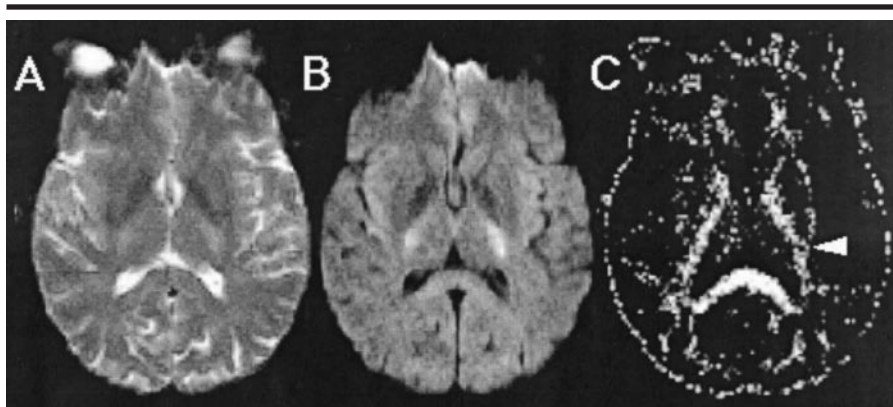


**Figure 4.** Images obtained axially in a 42-year-old woman 9.5 hours after the onset of symptoms. The imaging parameters were 6,000/118 with a  $b$  value of 1,221 sec/mm<sup>2</sup>. *A*, T2-weighted echo-planar image (the image obtained with low  $b$  value). *B*, Isotropic diffusion-weighted image. *C*, Fractional anisotropy map. The conspicuity of the ischemic zone is greatest in *B* owing to the homogeneity of the background. In *C*, the white matter in the area of ischemia (arrowhead) shows a decrease in fractional anisotropy.

**TABLE 2**  
Changes in ADC and Fractional Anisotropy in Normal and Ischemic Gray Matter and White Matter

**A: Mean (SD) Values of 2 × 2 ROIs**

Measurement	Normal GM	Ischemic GM	Normal WM	Ischemic WM
ADC	0.73 (0.12)	0.46 (0.13)	0.74 (0.17)	0.54 (0.21)
FA	0.35 (0.12)	0.36 (0.12)	0.52 (0.14)	0.45 (0.15)

**B: Significance between Populations**

Measurement	Normal Differences		Ischemic Differences	
	GM vs WM		GM vs GM Infarct	WM vs WM Infarct
ADC	.89		<.001	<.001
FA	<.001		.63	.01

Note.—FA = fractional anisotropy, GM = gray matter, WM = white matter.

The statistical analysis was either non-parametric two-tailed Wilcoxon signed rank tests for paired comparisons or Student  $t$  tests, assuming heteroscedasticity for nonpaired comparisons. Wilcoxon signed rank tests were used for comparing differences in anisotropy, eigenvalues, and ADC between ipsilateral and contralateral hemispheres. Student  $t$  tests were used for computing the statistical significance of differences in fractional anisotropy, eigenvalues, and ADC values between normal white and gray matter and cerebrospinal fluid. A one-way analysis of variance was performed followed by a two-tailed Student  $t$  test, assuming heteroscedasticity to compare group differences between  $\lambda_1$ ,  $\lambda_2$ , and  $\lambda_3$ . An F test was performed to compare variances between gray and white matter eigenvalues. A  $P$  value less than .05 was considered to indicate a statistically significant difference.

## RESULTS

Figure 1 displays a representative isotropic diffusion-weighted image, an ADC image, and a fractional anisotropy image for the healthy volunteer who underwent imaging with use of 30 signals acquired for one section. The white matter has a higher degree of fractional anisotropy than the gray matter.

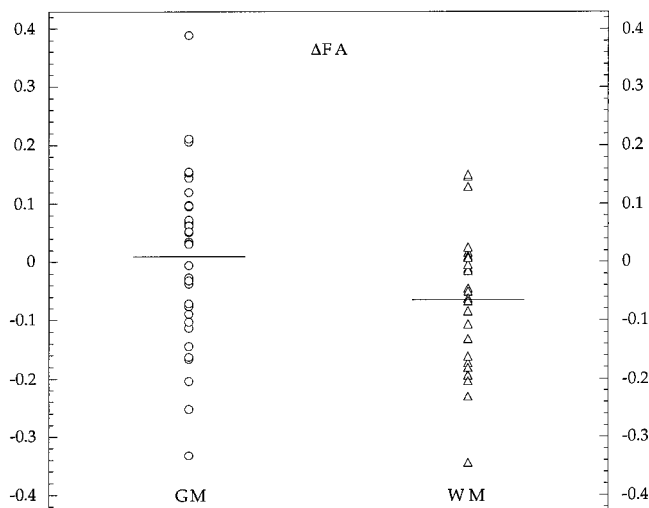
The mean of the eigenvalues measured from ROIs placed in the splenium of the corpus callosum and left forceps major in Figure 1 were used for the Monte Carlo simulations. The results of the Monte Carlo simulations are shown in Figure 2. The corpus callosum had a higher level of anisotropy than the left forceps major, with a resultant higher CNR when the simulated corpus callosum tissue was compared with simulated isotropic tissue. On the basis of empiric measurements,

we estimated an SNR of 20 for our clinically acquired diffusion data. At our SNR, these three metrics performed approximately the same. However, at a higher SNR, volume ratio has poorer performance than the other two metrics. To be consistent, we chose to use fractional anisotropy for measuring changes in anisotropy because it provided the highest CNR of the metrics studied in both the corpus callosum and the left forceps major (Fig 2).

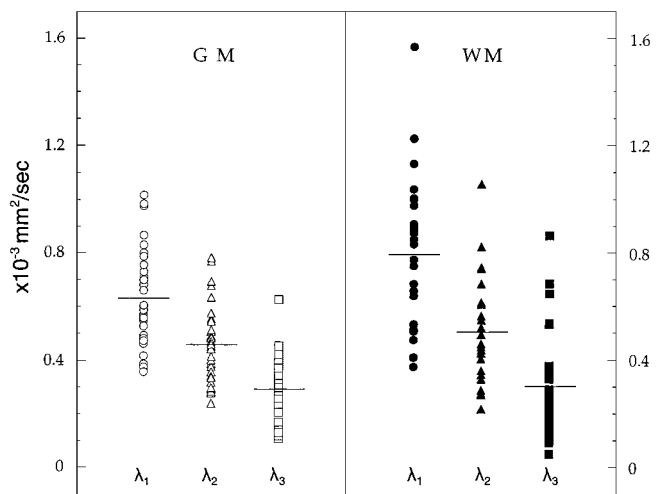
Table 1 summarizes the trace ADC values, fractional anisotropy index values, and eigenvalues measured in the healthy volunteer in 2 × 2 ROIs. ADC values in gray matter, white matter, and cerebrospinal fluid are stable at repeated measures. Moving from cerebrospinal fluid to normal gray matter to normal white matter, a stepwise increase in anisotropy is observed. While white matter is much more anisotropic than gray matter or cerebrospinal fluid, deep gray matter voxels are not completely isotropic. Gray matter has twice the fractional anisotropy value of isotropic cerebrospinal fluid (Table 1), a significant difference ( $P < .001$ ). The difference between gray matter and white matter fractional anisotropy values was significant ( $P < .001$ ). For ADC, the difference between gray matter and white matter was also significant ( $P = .003$ ).

Figure 3 shows the eigenvalues of the normal contralateral regions in the patients with acute stroke. Using a one-way analysis of variance, we found that the eigenvalues were all significantly different ( $P < .001$ ) from each other in both normal gray matter and normal white matter. Performing a two-tailed heteroscedastic Student  $t$  test further demonstrated a significant difference between all pairs of eigenvalues ( $P < .001$ ). However, this difference may be due to noise-related bias and variance (25). Monte Carlo simulations predicted that given the SNR of 20 and assuming true eigenvalues of 1.0, 0.7, and  $0.7 \times 10^{-3}$  mm<sup>2</sup>/sec, differences in the second and third eigenvalues greater than 0.5 were needed to substantiate non-axisymmetry. Consistent with previous reports (25), eigenvalues from normal white matter have slightly larger variability than those from normal gray matter. However, the differences in variances between gray and white matter for our data set were not significant, except for  $\lambda_1$  (F test for  $\lambda_1$ ,  $P = .006$ ;  $\lambda_2$ ,  $P = .08$ ; and  $\lambda_3$ ,  $P = .08$ ).

Figure 4 displays T2-weighted, diffusion-weighted, and fractional anisotropy images acquired at an SNR of 20 in a representative case of acute ischemic



**Figure 5.** Graph shows fractional anisotropic differences ( $\Delta FA$ ) between ischemic gray matter (GM) and ischemic white matter (WM) and normal contralateral regions. Regions that were abnormal on initial diffusion-weighted images and infarcted at follow-up examination and their contralateral regions were selected. The values plotted are the difference between the abnormal and contralateral values in unitless dimensions. The change in white matter was significant ( $P = .01$ ). The horizontal lines indicate the sample means.



**Figure 6.** Graph shows eigenvalues in abnormal regions in patients with acute ischemia. The horizontal lines indicate the sample means. Abnormal mean  $\lambda_1$ ,  $\lambda_2$ , and  $\lambda_3$  values are still significantly different from each other in both gray matter (GM) and white matter (WM). With the exception of the significance between  $\lambda_2$  and  $\lambda_3$  in white matter, the level of significance between the other eigenvalues is  $P$  less than .001 as determined by using heteroscedastic Student  $t$  tests. In the case of  $\lambda_2$  and  $\lambda_3$  for white matter, the differences are significant at  $P$  equals .001.

stroke. Consistent with expectations from results of Monte Carlo simulations (Fig 2), a higher CNR was seen in the high-SNR brain image from the healthy volunteer (Fig 1) than in the ischemic brain image (Fig 4). Nonetheless, even at an SNR of 20, the decreased anisotropy in the region of decreased ADC was clearly evident as an area of hypointensity.

Table 2 summarizes the results from patients presenting with acute ischemic stroke. There was a significant decrease in ADC between ischemic brain and normal brain, for both white and gray matter ischemia ( $P < .001$ ). A significant decrease in fractional anisotropy ( $P = .01$ ) between the contralateral and ipsilateral hemispheres was detected in only white matter and not in gray matter ( $P = .63$ ). Figure 5 displays the differences between abnormal and contralateral fractional anisotropy values for all of the patients. Figure 6 shows the eigenvalues measured in the abnormal ischemic ROIs.  $F$  tests comparing the observed variabilities between gray matter and white matter ischemic tissue yielded  $P$  values of .005 for  $\lambda_1$ , .06 for  $\lambda_2$ , and .003 for  $\lambda_3$ .

In Figure 7, the difference in eigenvalues between the ischemic and normal contralateral hemispheres is plotted. A significant decrease for the first ( $P < .001$  for both gray and white matter) and second ( $P < .001$  for gray matter and  $P = .001$  for white matter) eigenvalues was

found. A significant decrease in the third eigenvalue ( $\lambda_3$ ) was found in gray matter ( $P < .001$ ) and in white matter ( $P = .03$ ).

## DISCUSSION

While the focus of recent clinical studies (1,2,7,10,11,15-17) appropriately has been on the decrease in the trace or single-direction ADC in acute cerebral ischemia, our results confirm those of earlier reports of changes in anisotropy in animal models of cerebral ischemia (30) and in patients with chronic stroke (26,27). Our data extend previous work by documenting acute changes in the eigenvalues of white and gray matters, thus demonstrating that measurement of the full tensor can provide additional microanatomic information in human tissue.

Our results also confirm the results of earlier work (25,31,40) on the choice of scalar metric and extend this work by identifying fractional anisotropy as the metric with the best performance characteristics over the range of SNRs available to us. We now use fractional anisotropy as our anisotropy metric of choice for investigation of changes in anisotropy.

As Tables 1 and 2 and Figures 1 and 4 demonstrate, anisotropy maps can be used to differentiate clearly between gray and white matter. The distance scale to which

our sequence is sensitive can be derived from the Einstein relation, which states that the time scale ( $\Delta$ ) is sensitive to diffusion on the length scale,  $L = (2D\Delta)^{1/2}$ . For our implementation,  $L = 11 \mu\text{m}$ , assuming  $D = 1.2 \times 10^{-3} \text{ mm}^2/\text{sec}$ , the average  $\lambda_1$  measured in the white matter in the normal hemisphere for the patient population in our study. This distance scale is comparable to typical neuroglial cell soma diameters of 7-15  $\mu\text{m}$  (42). The resultant images are different from those obtained with conventional MR imaging in that they are based on microscopic diffusion properties rather than on relaxation properties.

The exact mechanisms underlying the ADC changes in ischemic brain remain controversial. Anisotropy has not been a major component of the proposed models to date. However, such information may prove useful as the models used to understand the ADC changes in early cerebral ischemia are refined. For example, the ADC decrease in ischemic white matter was largest in  $\lambda_1$ , the direction of which has been shown to align with white matter tracts (27). One thus can speculate that ADC decreases might be along the long axis of the white matter fiber tracts.

Our data with a high SNR of 65 demonstrated a significant difference between  $\lambda_2$  and  $\lambda_3$  in nonischemic gray matter ( $P = .001$ ) and nonischemic white matter ( $P =$

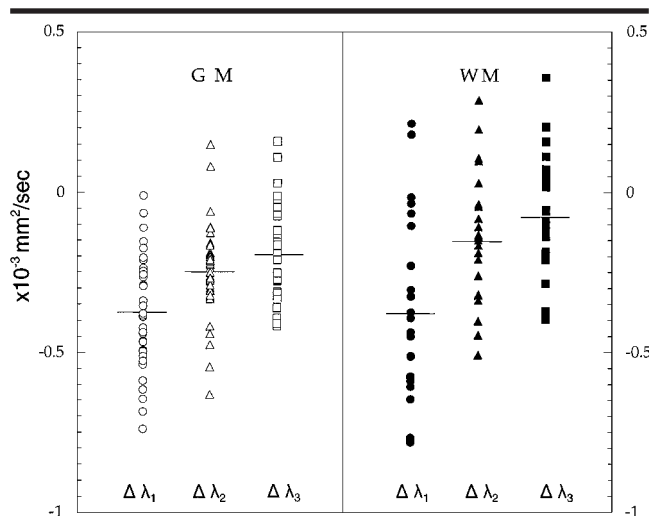


**Figure 7.** Graph shows changes in  $\lambda_1$ ,  $\lambda_2$ , and  $\lambda_3$  during ischemia in gray matter (GM) and white matter (WM). The horizontal lines indicate the sample means. All eigenvalues have significant changes ( $P \leq .001$ ), with the exception of  $\lambda_3$  in white matter ( $P = .03$ ) as determined by using a Wilcoxon signed rank test. The plotted data points are the difference between eigenvalues measured in the ipsilateral and contralateral hemispheres.

.01). These findings of nonaxisymmetry have also been detected by other groups (25). Furthermore, our data indicate that during ischemia,  $\lambda_2$  and  $\lambda_3$  may behave differently, which suggests that the assumption of axisymmetry may prevent an accurate description of water diffusion behavior in acute cerebral ischemia. Therefore, it may be prudent to acquire the full six diffusion directions in tensor studies.

As can be seen in Figure 6, the variance in the ischemic white matter ROIs is quite high, which suggests that there may be some biologic heterogeneity. The changes we see in anisotropy may occur to a different degree in different white matter locations; further subset analyses await collection of additional data. While the anisotropy maps were sensitive to changes in white matter anisotropy, we found the visual conspicuity of early ischemia is still highest on the trace diffusion-weighted images. These images normally have little or no gray-white contrast. In addition, on the basis of our Monte Carlo simulations, fluctuations in noise had greater effects on anisotropy metrics than they do on ADC values.

Anisotropy maps provide useful information not captured in ADC values. One example is the ability to differentiate between white and gray matter in cases in which the biology of ischemic injury may well differ. Water can diffuse into the neuronal cell bodies that make up gray matter through neurotransmitter-gated

ion channels, synapses, and a concentration of voltage-gated ion channels not found in white matter. The dense arrays of parallel white matter tracts create a structured extracellular space that differs substantially from that found in the meshwork of gray matter. It may be that diffusion tensor changes in shape are more evident in white matter than in gray matter owing to the greater structure and hence anisotropy present in normal white matter as compared with normal gray matter.

Nonetheless, careful evaluation of anisotropy metrics is needed. There are at least three causes for variability: (a) anisotropy metrics, themselves, are sensitive to noise contamination (Fig 2); (b) anisotropy itself is quite variable throughout white matter (Fig 1); (c) just as ADC values first decrease and later pseudo-normalize, anisotropy values may also vary in different stages of stroke. These many causes of variability may contribute to the fractional anisotropy changes in our sample size. With such high variability, even conspicuous changes reach only moderate significance ( $P = .01$ ). Changes in anisotropy and the eigenvalues that characterize the full diffusion tensor therefore need further investigation.

In conclusion, our data demonstrate that full-tensor imaging is feasible in the clinical setting of stroke imaging. Even at the low SNR available clinically, useful maps of anisotropy metrics can be gener-

ated. Most important, human acute cerebral ischemia causes changes in the anisotropy or shape of the diffusion tensor in white matter. Further investigation into such changes may help clarify the nature of the biophysical changes in acute cerebral ischemia and eventually shed further light on the pathophysiology of this leading cause of morbidity and mortality.

## References

1. Warach S, Chien D, Li W, Ronthal M, Edelman RR. Fast magnetic resonance diffusion-weighted imaging of acute human stroke. *Neurology* 1992; 42:1717-1723.
2. Warach S, Gaa J, Siewert B, Wielopolski P, Edelman R. Acute human stroke studied by whole brain echo planar diffusion-weighted magnetic resonance imaging. *Ann Neurol* 1995; 37:231-241.
3. Sorensen AG, Buonanno FS, Gonzalez RG, et al. Hyperacute stroke: evaluation with combined multisection diffusion-weighted and hemodynamically weighted echoplanar MR imaging. *Radiology* 1996; 199:391-401.
4. Le Bihan D, Breton E, Lallemand D, Grenier P, Cabanis E, Laval-Jeantet M. MR imaging of intravoxel incoherent motions: application to diffusion and perfusion in neurologic disorders. *Radiology* 1986; 161:401-407.
5. Thomsen C, Henriksen O, Ring P. In vivo measurement of water self-diffusion in the human brain by magnetic resonance imaging. *Acta Radiol* 1987; 28:353-361.
6. Le Bihan D, Breton E, Lallemand D, Aubin ML, Vignaud J, Laval-Jeantet M. Separation of diffusion and perfusion in intravoxel incoherent motion MR imaging. *Radiology* 1988; 168:497-505.
7. Hajnal J, Doran M, Hall A, et al. MR imaging of anisotropically restricted diffusion of water in the nervous system: technical, anatomic, and pathologic considerations. *J Comput Assist Tomogr* 1991; 15:1-18.
8. Tsuruda JS, Chew WM, Moseley ME, Norman D. Diffusion-weighted MR imaging of extraaxial tumors. *Magn Reson Med* 1991; 19:316-320.
9. Chien D, Kwong KK, Gress DR, Buonanno FS, Buxton RB, Rosen BR. MR diffusion imaging of cerebral infarction in humans. *AJNR* 1992; 13:1097-1102.
10. Welch K, Windham J, Knight R, et al. A model to predict the histopathology of human stroke using diffusion and T2-weighted magnetic resonance imaging. *Stroke* 1995; 26:1983-1989.
11. Lutsep HL, Albers GW, De Crespigny A, Kamat GN, Marks MP, Moseley ME. Clinical utility of diffusion-weighted magnetic resonance imaging in the assessment of ischemic stroke. *Ann Neurol* 1997; 41:574-580.
12. Takeda K, Nomura Y, Sakuma H, Tagami T, Okuda Y, Nakagawa T. MR assessment of normal brain development in neonates and infants: comparative study of T1- and diffusion-weighted images. *J Comput Assist Tomogr* 1997; 21:1-7.
13. Brunberg JA, Chenevert TL, McKeever PE, et al. In vivo MR determination of water diffusion coefficients and diffusion anisotropy: correlation with structural alter-

- ation in gliomas of the cerebral hemispheres. *AJNR* 1995; 16:361-371.
14. de Crespigny AJ, Marks MP, Enzmann DR, Moseley ME. Navigated diffusion imaging of normal and ischemic human brain. *Magn Reson Med* 1995; 33:720-728.
  15. Baird AE, Benfield A, Schlaug G, et al. Enlargement of human cerebral ischemic lesion volumes measured by diffusion-weighted magnetic resonance imaging. *Ann Neurol* 1997; 41:581-589.
  16. Lovblad KO, Baird AE, Schlaug G, et al. Ischemic lesion volumes in acute stroke by diffusion-weighted magnetic resonance imaging correlate with clinical outcome. *Ann Neurol* 1997; 42:164-170.
  17. Schlaug G, Siewert B, Benfield A, Edelman RR, Warach S. Time course of the apparent diffusion coefficient (ADC) abnormality in human stroke. *Neurology* 1997; 49:113-119.
  18. Ulug AM, Beauchamp N, Bryan RN, van Zijl PCM. Absolute quantitation of diffusion constants in human stroke. *Stroke* 1997; 28:483-490.
  19. Chien D, Buxton RB, Kwong KK, Rosen BR. MR diffusion imaging of the human brain. *J Comput Assist Tomogr* 1990; 14:514-520.
  20. Chenevert TL, Brunberg JA, Pipe JG. Anisotropic diffusion in human white matter: demonstration with MR techniques in vivo. *Radiology* 1990; 177:401-405.
  21. Douek P, Turner R, Pekar J, Patronas N, Le Bihan D. MR color mapping of myelin fiber orientation. *J Comput Assist Tomogr* 1991; 15:923-929.
  22. Sakuma H, Nomura Y, Takeda K, et al. Adult and neonatal human brain: diffusional anisotropy and myelination with diffusion-weighted MR imaging. *Radiology* 1991; 180:229-233.
  23. Coremans J, Luypaert R, Verhelle F, Stadnik T, Osteaux M. A method for myelin fiber orientation mapping using diffusion-weighted MR images. *Magn Reson Imaging* 1994; 12:443-454.
  24. Nomura Y, Sakuma H, Takeda K, Tagami T, Okuda Y, Nakagawa T. Diffusional anisotropy of the human brain assessed with diffusion-weighted MR: relation with normal brain development and aging. *AJNR* 1994; 15:231-238.
  25. Pierpaoli C, Jezzard P, Basser PJ, Barnett A, Di Chiro G. Diffusion tensor MR imaging of the human brain. *Radiology* 1996; 201:637-648.
  26. Pierpaoli C, Penix L, De Graba T, Basser PJ, Di Chiro G. Identification of fiber degeneration and organized gliosis in stroke patients by diffusion tensor MRI (abstr). In: Proceedings of the Fourth Meeting of the International Society for Magnetic Resonance in Medicine. Berkeley, Calif: International Society for Magnetic Resonance in Medicine, 1996; 563.
  27. Makris N, Worth AJ, Sorensen AG, et al. Morphometry of in vivo human white matter association pathways with diffusion-weighted magnetic resonance imaging. *Ann Neurol* 1997; 42:951-962.
  28. van Gelderen P, de Vleeschouwer MHM, Des Pres D, Pekar J, van Zijl PCM, Moonen CTW. Water diffusion and acute stroke. *Magn Reson Med* 1994; 31:154-163.
  29. Moonen CT, Pekar J, de Vleeschouwer MH, van Gelderen P, van Zijl PC, Des Pres D. Restricted and anisotropic displacement of water in healthy cat brain and in stroke studied by NMR diffusion imaging. *Magn Reson Med* 1991; 19:327-332.
  30. Kajima T, Azuma K, Itoh K, et al. Diffusion anisotropy of cerebral ischemia. *Acta Neurochir Suppl (Wien)* 1994; 60:216-219.
  31. Pierpaoli C, Basser PJ. Toward a quantitative assessment of diffusion anisotropy. *Magn Reson Med* 1996; 36:893-906.
  32. Einstein A. Investigations on the theory of the Brownian movement. New York, NY: Dover Publications, 1956.
  33. Tanner JE, Stejskal EO. Restricted self-diffusion of protons in colloidal systems by the pulsed-gradient, spin-echo method. *J Chem Phys* 1968; 49:1768-1777.
  34. Stejskal E, Tanner J. Spin diffusion measurements: spin echoes in the presence of a time-dependent field gradient. *J Chem Phys* 1965; 42:288-292.
  35. McKinstry RC, Weiskoff RM, Belliveau JW, et al. Ultrafast MR imaging of water mobility: animal models of altered cerebral perfusion. *JMRI* 1992; 2:377-384.
  36. Basser PJ, Mattiello J, Le Bihan D. MR diffusion tensor spectroscopy and imaging. *Biophys J* 1994; 66:259-267.
  37. Mattiello J, Basser PJ, Le Bihan D. Analytical expressions for the *b* matrix in NMR diffusion imaging and spectroscopy. *J Magn Reson* 1994; 108:131-141.
  38. Basser PJ, Mattiello J, Le Bihan D. Estimation of the effective self-diffusion tensor from the NMR spin echo. *J Magn Reson* 1994; 103:247-254.
  39. Mattiello J, Basser PJ, Le Bihan D. The *b* matrix in diffusion tensor echo-planar imaging. *Magn Reson Med* 1997; 37:292-300.
  40. Basser PJ, Pierpaoli C. Microstructural and physiological features of tissues elucidated by quantitative-diffusion tensor MRI. *J Magn Reson* 1996; 111:209-219.
  41. Henkelman RM. Measurement of signal intensities in the presence of noise in MR images. *Med Phys* 1985; 12:232-233.
  42. Gray H. Anatomy of the human body. 37th ed. Edinburgh, UK: Longman, 1989; 875.